

Dynamic vortex Mott transition in triangular superconducting arrays

Zi-Xi Pei(裴子玺), Wei-Gui Guo(郭伟贵), and Xiang-Gang Qiu(邱祥冈)

Citation: Chin. Phys. B, 2022, 31 (**3**): 037404. DOI: 10.1088/1674-1056/ac3cb1
Journal homepage: http://cpb.iphy.ac.cn; http://iopscience.iop.org/cpb

What follows is a list of articles you may be interested in

Wire network behavior of superconducting films with lower symmetrical mesoscopic hole arrays

Wei-Gui Guo(郭伟贵), Zi-Xi Pei(裴子玺), and Xiang-Gang Qiu(邱祥冈)
Chin. Phys. B, 2022, 31 (**3**): 037405. DOI: 10.1088/1674-1056/ac43af

Design, fabrication, and characterization of Ti/Au transition-edge sensor with different dimensions of suspended beams

Hong-Jun Zhang(张宏俊), Ji Wen(文继), Zhao-Hong Mo(莫钊洪), Hong-Rui Liu(刘鸿瑞), Xiao-Dong Wang(汪小东), Zhong-Hua Xiong(熊忠华), Jin-Wen Zhang(张锦文), and Mao-Bing Shuai(帅茂兵)
Chin. Phys. B, 2021, 30 (**11**): 117401. DOI: 10.1088/1674-1056/abff20

Phase-field simulation of superconductor vortex clustering in the vicinity of ferromagnetic domain bifurcations

Hasnain Mehdi Jafri, Jing Wang(王静), Chao Yang(杨超), Jun-Sheng Wang(王俊升), and Hou-Bing Huang(黄厚兵)
Chin. Phys. B, 2020, 29 (**12**): 127402. DOI: 10.1088/1674-1056/abb22c

Recent advances in generation of terahertz vortex beams andtheir applications

Honggeng Wang(王弘耿), Qiying Song(宋其迎), Yi Cai(蔡懿), Qinggang Lin(林庆钢), Xiaowei Lu(陆小微), Huangcheng Shangguan(上官煌城), Yuexia Ai(艾月霞), Shixiang Xu(徐世祥)
Chin. Phys. B, 2020, 29 (**9**): 097404. DOI: 10.1088/1674-1056/aba2df

Time-dependent Ginzburg-Landau equations for multi-gap superconductors

Minsi Li(李敏斯), Jiahong Gu(古家虹), Long Du(杜龙), Hongwei Zhong(钟红伟), Lijuan Zhou(周丽娟), Qinghua Chen(陈庆华)
Chin. Phys. B, 2020, 29 (**3**): 037401. DOI: 10.1088/1674-1056/ab69ef

---

Dynamic vortex Mott transition in triangular superconducting arrays

Zi-Xi Pei(裴子玺)[1,2], Wei-Gui Guo(郭伟贵)[1,2], and Xiang-Gang Qiu(邱祥冈)[1,2,3,†]

[1] *Beijing National Laboratory for Condensed Matter Physics, Institute of Physics, Chinese Academy of Sciences, Beijing* 100190, *China*
[2] *School of Physical Sciences, University of Chinese Academy of Sciences, Beijing* 100049, *China*
[3] *Collaborative Innovation Center of Quantum Matter, Beijing* 100084, *China*

(Received 4 November 2021; revised manuscript received 22 November 2021; accepted manuscript online 24 November 2021)

The proximity-coupled superconducting island arrays on a metallic film provide an ideal platform to study the phase transition of vortex states under mutual interactions between the vortex and potential landscape. We have developed a top-down microfabrication process for Nb island arrays on Au film by employing an Al hard mask. A current-induced dynamic vortex Mott transition has been observed under the perpendicular magnetic fields of f magnetic flux quantum per unit cell, which is characterized by a dip-to-peak reversal in differential resistance $\mathrm{d}V/\mathrm{d}I$ vs. f curve with the increasing current. The $\mathrm{d}V/\mathrm{d}I$ vs. I characteristics show a scaling behavior near the magnetic fields of $f = 1/2$ and $f = 1$, with the critical exponents ε of 0.45 and 0.3, respectively, suggesting different universality classes at these two fields.

Keywords: microfabrication, superconducting array, Mott transition

PACS: 74.25.Uv, 74.45.+c, 81.16.Rf **DOI:** 10.1088/1674-1056/ac3cb1

1. Introduction

Artificially fabricated superconducting systems have attracted much interest both in the study of vortex dynamics and applications because of its flexibility to tune the pinning and mutual interaction of vortices. One of such systems is the superconducting island arrays placed on normal metal films composing superconductor–normal-metal–superconductor (SNS) structure.[1–5] With the proximity effect coupled superconducting island arrays, the superconducting vortices in this system[6] result in spatially arranged superconducting order parameters and move with a phase slip mechanism in the 'eggcrate potential' created by the underlying arrays. The pinning sites of the vortices are located between the islands where the potential minima exist.[7–9] At some special magnetic fields when the vortex lattice is commensurate with the arrays, the occupation of the pinning sites prevents the motion of the vortices and a vortex Mott insulating state emerges.[10]

In the previous works, the current-induced dynamic vortex Mott transition was firstly observed[3,5] in the square superconducting island arrays under a perpendicular magnetic field of f flux quantum per unit cell. Different from the vortex depinning transition where the dips in the resistance versus magnetic field (R–f) curve disappear,[7,11] in the case of a dynamic vortex Mott transition a dip-to-peak reversal of the differential resistance versus magnetic field ($\mathrm{d}V/\mathrm{d}I$–f) curve near a rational f was observed while the dips in the R–f curve existed during the transition. The transition is described by a scaling behavior resembling the electronic Mott transition and characterized by a single critical exponent ε. The simulations of Josephson junction model with the same structure give the same critical exponent.[12,13] But in the simulation of a long-range Coulomb interaction between the vortices,[14] the scaling analysis gives a different critical exponent. It was concluded that the critical exponent is influenced by the interaction form between the vortices. As the potential landscape induced by the underlying arrays also influences the transition, it is interesting to investigate the transition in superconducting island arrays with different structures.

In this paper, current induced dynamic vortex Mott transition in triangular superconducting arrays has been studied. The $\mathrm{d}V/\mathrm{d}I$–f curve shows that the dip-to-peak reversal emerges near the magnetic fields of $f = 1$ and $f = 1/2$. Detailed measurements of $\mathrm{d}V/\mathrm{d}I$–f near these two fields were performed to investigate the possible vortex Mott transition. It is found that the $\mathrm{d}V/\mathrm{d}I$–I curves can be scaled as what is expected from a vortex Mott transition. The scaling behavior near the critical currents is the same as that in the square arrays[3] but with different critical exponents ε. For the case of $f = 1/2$, $\varepsilon = 0.45$ and for $f = 1$, $\varepsilon = 0.3$, suggesting that in the current system, the vortex Mott transitions at integer f and fractional f belong to different universality classes.

2. Experiment

There are two different ways for the fabrication of the Nb island arrays. One is a bottom-up approach where the array is first exposed on a photoresist, followed by the deposition of Nb film on the exposed resist mask. Previous works[2,3,5,15] used this bottom-up microfabrication process because it is a convenient two-step approach. But such a bottom-up approach has disadvantages. For example, the resist residues at the exposed area may affect the Nb–Au interface and the shape of the

†Corresponding author. E-mail: xgqiu@iphy.ac.cn

© 2022 Chinese Physical Society and IOP Publishing Ltd

array top can not be fully controlled. Besides, to avoid deposition on the resist sidewalls, a long distance between the source and the sample is necessary for the instrument. To avoid the above mentioned disadvantages, we developed a top-down approach to fabricate the superconducting island arrays. Before the microfabrication, the Au and Nb layers were deposited in a high vacuum chamber in which there were Au and Nb targets. As shown in Fig. 1(a), the standard top-down approach includes an electron beam lithograph (EBL) process for patterning the PMMA resist arrays as a mask on the top of the Nb film. Then a reactive ion etching (RIE) process is followed to remove the uncovered Nb film. After dissolving the resist in acetone, the sample was obtained. The EBL exposing area of the PMMA resist in this method is shown in Fig. 1(b). As the exposed area has an irregular shape, the residual resist arrays after the EBL process can hardly keep a circular shape because of the optical proximity effect. Here we developed a new method on the basis of the standard top-down approach. As shown in Fig. 1(c), the EBL process was used to create the resist mask not for etching but for Al deposition. Such that the exposed area was circular arrays, as shown in Fig. 1(d). By doing so, the influence of the optical proximity effect for the island shape can be avoided. The Al island arrays were fabricated after the electron beam deposition (EBD) and a PMMA lift-off process, which was then served as a hard mask. We chose Al as the hard mask because in the RIE process of Nb the consumption of Al mask can be ignored and it can be easily removed. Then the Nb film was etched with the mixture of Ar and SF_6 as working gas. As the etching speed of Au film is far lower than that of Nb with the working gas, it is easy to control the etching time so that the uncovered Nb layer was completely etched without damaging the Au layer. Finally the Al mask was washed out with weak alkaline solution. With this top-down microfabrication approach, we successfully prepared high quality samples with cylindric shaped island arrays.

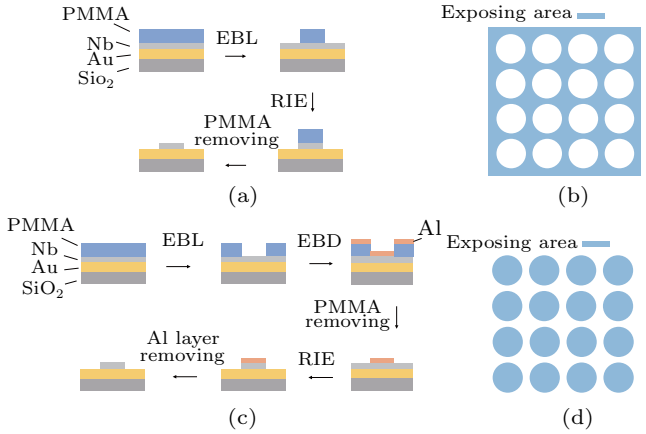


Fig. 1. (a) The standard top-down approach for microfabrication. (b) The exposing area of patterning the photoresist as a mask for etching. (c) The improved microfabrication process for a better island shape. (d) The exposing area of patterning the photoresist as a mask for deposition.

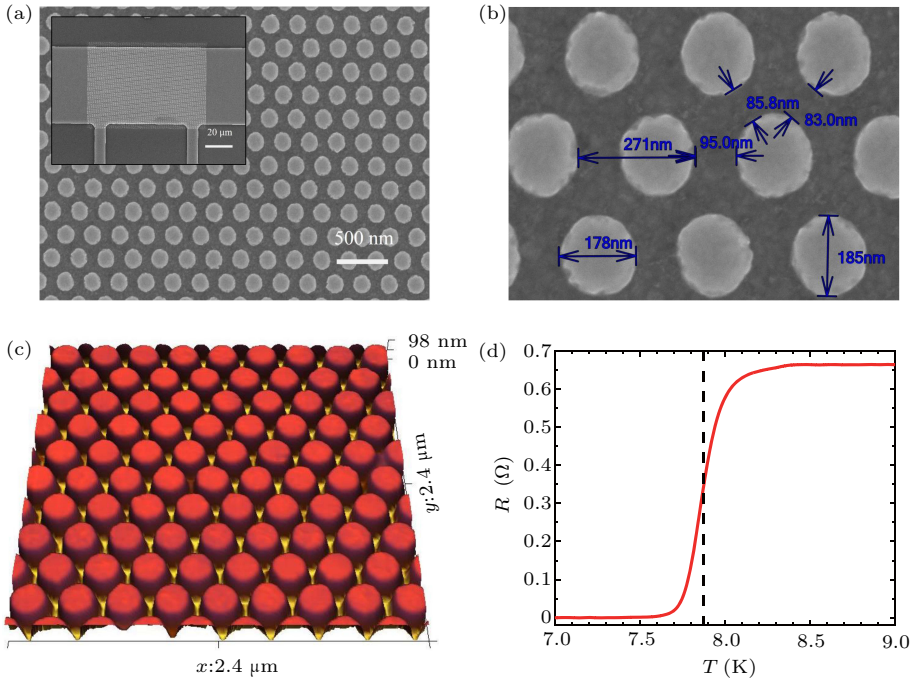


Fig. 2. (a) Scanning electron microscopy image of the triangular Nb island arrays on Au film, the insert is the bridge for transport measurements. (b) A magnified scanning electron microscopy image of the same sample. (c) Atom force microscopy image of the same sample. (d) The resistance versus temperature curve near the critical temperature.

The 90 nm Nb and 50 nm Au layers were deposited on 1×1 cm^2 Si/SiO_2 substrate with magnetic sputtering process. The UV exposure was used to pattern a resist mask then the micro-bridge for transport measurements was created by the RIE processes. The central area of the bridge is 60×60 μm^2 with four terminals as electrods. Then a EBL process was used to pattern the 90×65 μm^2 resist mask covering the bridge center. After that, the hard mask was created by Al deposi-

tion and the PMMA lift-off process. Then the sample was etched by a RIE process to remove the part of Nb layer uncovered by the Al mask. After the etching, the hard mask can be washed out by AZ 300MIF solution. As shown in the insert of Fig. 2(a), the patterned area of 90×65 μm^2 was at the center of the bridge, covering an area of 60×60 μm^2. As shown in Figs. 2(a)–2(c), each Nb island has a cylindrical shape, with a diameter $d = 180$ nm, a height $h = 90$ nm, and a period $a = 270$ nm.

All the transport measurements were carried out in the Quantum Design PPMS-9. The applied DC current was introduced by the Keithley Model 6221 DC current source and the DC voltage was measured by the Keithley Model 2182 nanovoltmeter. The applied AC current was introduced by the Lakeshore Model 370 AC resistance bridge, which was also used to measure the differential resistance ($\mathrm{d}V/\mathrm{d}I$). The critical temperature of the sample, determined as the 50% of the nomal state (9 K) resistance, was about 7.9 K as shown in Fig. 2(d). The high critical temperature indicates that the coupling energy E_J between the superconducting arrays is strong enough to obtain a high vortex pinning potential for forming the vortex Mott insulator state.[2,16]

3. Results and discussion

The resistance versus magnetic field (R–f) and the differential resistance versus magnetic field ($\mathrm{d}V/\mathrm{d}I$–f) were measured simultaneously at 2 K with the transporting current from 0.4 mA to 2.2 mA. Here the magnetic field is represented by $f = B/B_0$, which is the number of the magnetic flux quantum per unit cell of the array, where $B_0 = \Phi_0/(\frac{\sqrt{3}}{4}a^2)$ and $\Phi_0 = \frac{h}{2e}$ is the magnetic flux quantum. As shown in Fig. 3(a), several resistance minima emerge near the commensurate fields $f = 0, 1/4, 1/3, 3/8, 1/2, 5/8, 2/3, 3/4, 1$. Those dips indicate the minima of the ground state energy of this system, which can be calculated from the RCSJ model[17] and has been observed in many previous works.[15,18] The vortex lattice at those fields is commensurate with the underlying superconducting island arrays and in a pinned vortex insulating state. The depths of those dips reflect the pinning strength at the commensurate fields and with the increase of the applied current, the dips at the weakly pinned commensurate fields disappear. As can be seen in Fig. 3(b), the $\mathrm{d}V/\mathrm{d}I$–f curves also show minima near the same magnetic fields of $f = 0, 1/4, 1/3, 3/8, 1/2, 5/8, 2/3, 3/4, 1$. But with the increase of the applied current, the minima near the fields of $f = 1/2$ and $f = 1$ develop into maxima, which indicates that the vortices are in a metallic state. The same phenomenon has been observed in previous works,[11] which has been explained based on a vortex depinning mechanism. Since the vortex depinning would lead to the disappearance of the minima in the R–f curve, the existing minima at the fields of $f = 1/2$ and $f = 1$ of the R–f curve exclude the possibility of the vortex lattice depinning in this situation. The pinned vortex lattice transforms from an insulating state to a metallic one. As a result, the vortex lattice is expected to change from elasticity to plasticity.[19]

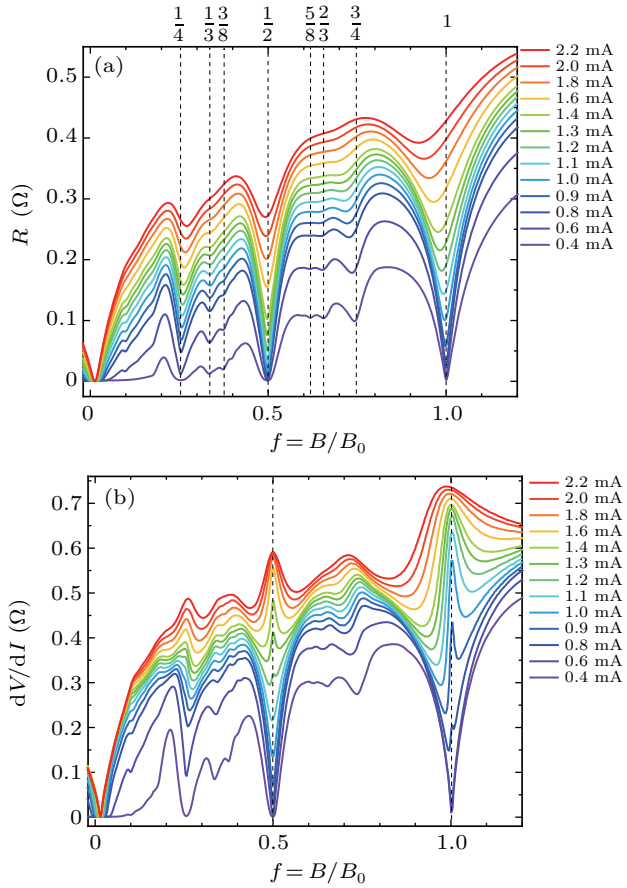


Fig. 3. (a) Resistance (R) versus magnetic field (f) curve with different applied currents, minima were found at $f = 0, 1/4, 1/3, 3/8, 1/2, 5/8, 2/3, 3/4, 1$. (b) Differential resistance ($\mathrm{d}V/\mathrm{d}I$) versus magnetic field (f) with different applied currents, minima were found at $f = 0, 1/4, 1/3, 3/8, 1/2, 5/8, 2/3, 3/4, 1$ with low applied current, dip-to-peak reversals occur at $f = 1/2$ and $f = 1$ with the increasing of the applied current. The R–f and $\mathrm{d}V/\mathrm{d}I$–f curves were measured simultaneously at 2 K with different currents.

We have measured the $\mathrm{d}V/\mathrm{d}I$–f curve near the magnetic fields of of $f = 1/2$ and $f = 1$ with more detailed measurements for applied currents of 10 μA interval, as shown in Figs. 4(a) and 4(b). The critical current of this transition, where the occurrence of a dynamic vortex Mott transition is determined by the disappearance of the minima in the $\mathrm{d}V/\mathrm{d}I$–f curve at commensurate fields $f = 1/2$ and $f = 1$, is marked with circles in Figs. 4(a) and 4(b). There are slight differences between the critical currents at magnetic fields higher and lower than the commensurate fields, written as $I_0^{\pm}$, we attribute this difference to the field dependent coupling energy E_J. Near the magnetic field $f = 1/2$, the critical current for $f < 1/2$ is $I_0^- = 1.02$ mA and for $f > 1/2$ is $I_0^+ = 1.07$ mA. Near the magnetic field $f = 1$, the critical current for $f < 1$ is $I_0^- = 0.65$ mA and for $f > 1$ is $I_0^+ = 0.68$ mA. The vor-

tex lattice state near the commensurate fields of $f = 1/2$ and $f = 1$ can be divided into three parts by the applied current. The vortex lattice is in a Mott insulating state for the applied current $I < I_0^{\pm}$, and the metallic state emerges when $I > I_0^{\pm}$. When the applied current is between I_0^+ and I_0^-, those two states coexist.[20]

To confirm that this current induced transition in our experiment is a dynamic vortex Mott transition, a scaling analysis[3] has been done. In the Hubbard model of electronic Mott transition, the insulating or metallic state of the system is determined by the Hubbard energy U due to the repulsion and the temperature T, with a critical point (U_C, T_C). Within the transition area, the deviation of U and T scales as $|U - U_C| \sim |T - T_C|^{\varepsilon}$. In the vortex system, the repulsion energy between vortices is tuned by the magnetic field. The motion of the vortex is driven by the applied current at this dynamic transition. So that the corresponding relations between the two transitions is $|U - U_C| \to |f - f_C|$ and $|T - T_C| \to |I - I_C|$. Treating $|f - f_C|$ as a perturbation and the differential resistance the scaling invariant quantity, the scaling relation is written as a universality form $\frac{dV}{dI} - \frac{dV}{dI}|_{(I=I_0^{\pm})} = F(\frac{|I-I_0^{\pm}|}{|f-f_C|^{\varepsilon}})$, where $F(x)$ is the scaling function, f_C is the commensurate field $1/2$ or 1, and ε is an adjustable parameter. The critical behavior is characteristized with the single exponent ε. We have measured the dV/dI–I curves with a smaller current interval near the magnetic fields $f = 1$ and $f = 1/2$ for the scaling analysis. As shown in Figs. 4(c) and 4(d), the critical exponent for the $f = 1/2$ case is $\varepsilon = 0.45$; and as shown in Figs. 4(e) and 4(f), the critical exponent for the $f = 1$ case is $\varepsilon = 0.3$. The critical exponents ε are different from the previous experiments, which suggests that the dynamic vortex Mott transitions in the triangular superconducting arrays belong to different universality classes.

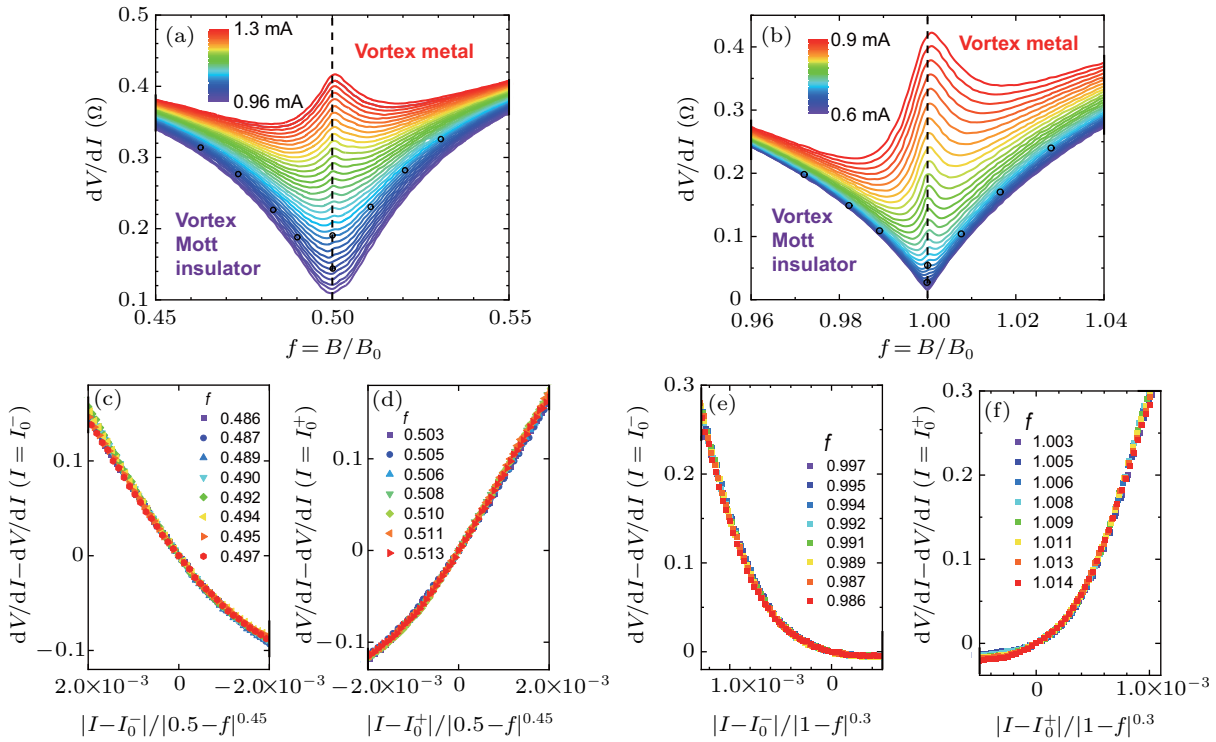


Fig. 4. (a) The dV/dI versus f curve measured near $f = 1/2$ with applied current from 0.96 mA to 1.3 mA. (b) dV/dI versus f curves measured near $f = 1$ with applied current from 0.6 mA to 0.9 mA. The figure contains the curves measured with different applied currents of 10 μA interval. The critical currents $I_0^{\pm}$ were determined where the dips at $f = 1/2$ and $f = 1$ disappeared. There are slight differences between critical currents below and above the two fields, written as I_0^- and I_0^+. For $f = 1/2$ case, $I_0^- = 1.02$ mA and $I_0^+ = 1.07$ mA. For $f = 1$ case, $I_0^- = 0.65$ mA and $I_0^+ = 0.68$ mA. (c) and (d) Scaling of $dV/dI - I$ curve measured at different fields near $f = 1/2$. The critical exponent $\varepsilon = 0.45$. (e) and (f) Scaling of dV/dI–I curves measured at different fields near $f = 1$. The critical exponent $\varepsilon = 0.3$.

4. Conclusion

We have developed a top-down micro-fabrication process to fabricate superconducting Nb island arrays on Au film by employing an Al hard mask. High quality samples with triangular Nb island arrays on Au film have been obtained. The relatively high superconducting critical temperature indicates a strong coupling between the superconducting islands. Commensurate fields in the field dependent resistance have been observed in integer and fraction f, which is consistent with the calculated results. A dip-to-peak reversal in the dV/dI–f curve has been found near the fields of $f = 1/2$ and $f = 1$. The scaling analysis reveals that the dip-to-peak reversals in the two fields are associated with the dynamic vortex Mott transition, the different critical exponents at these two fields suggest that the transitions belong to different universality classes.

Acknowledgments

X.G.Q. acknowledges the support from the National Natural Science Foundation of China (Grant Nos. 11974412 and 11774400) and the National Key R&D Program of China (Grant Nos. 2017YFA0302903 and 2018YFA0305703).

References

[1] Benz S P, Rzchowski M S, Tinkham M and Lobb C J 1990 *Phys. Rev. B* **42** 6165
[2] Eley S, Gopalakrishnan S, Goldbart P M and Mason N 2012 *Nat. Phys.* **8** 59
[3] Poccia N, Baturina T I, Coneri F, Molenaar C G, Wang X R, Bianconi G, Brinkman A, Hilgenkamp H, Golubov A A and Vinokur V M 2015 *Science* **349** 1202
[4] Lankhorst M and Poccia N 2016 *J. Supercond. Nov. Magn.* **29** 623
[5] Lankhorst M, Poccia N, Stehno M P, Galda A, Barman H, Coneri F, Hilgenkamp H, Brinkman A, Golubov A A, Tripathi V, Baturina T I and Vinokur V M 2018 *Phys. Rev. B* **97** 020504
[6] Newrock R S, Lobb C J, Geigenmüller U and Octavio M 2000 *Solid State Phys.* **54** 263
[7] Rzchowski M S, Benz S P, Tinkham M and Lobb C J 1990 *Phys. Rev. B* **42** 2041
[8] Dang E K F and Gyorffy B L 1993 *Phys. Rev. B* **47** 3290
[9] Yu W and Stroud D 1994 *Phys. Rev. B* **49** 6174
[10] Nelson D R and Vinokur V M 1993 *Phys. Rev. B* **48** 13060
[11] Jiang Z, Dikin D A, Chandrasekhar V, Metlushko V V and Moshchalkov V V 2004 *Appl. Phys. Lett.* **84** 5371
[12] Granato E 2018 *Phys. Rev. B* **98** 094511
[13] Granato E 2019 *Phys. Rev. B* **100** 104517
[14] Rademaker L, Vinokur V M and Galda A 2017 *Sci. Rep.* **7** 1
[15] Durkin M, Mondragon-Shem I, Eley S, Hughes T L and Mason N 2016 *Phys. Rev. B* **94** 024510
[16] Lobb C J, Abraham D W and Tinkham M 1983 *Phys. Rev. B* **27** 150
[17] Lin Y L and Nori F 2002 *Phys. Rev. B* **65** 214504
[18] Teitel S and Jayaprakash C 2016 *Phys. Rev. Lett.* **51** 1999
[19] Blatter G, Feigelman M V, Geshkenbein V B, Larkin A I and Vinokur V M 1994 *Rev. Mod. Phys.* **66** 1125
[20] Rozenberg M J, Chitra R and Kotliar G 1999 *Phys. Rev. Lett.* **83** 3498